P8.3 DESIGN AND PERFORMANCE CHARACTERISTICS OF THE NEW 9 M DUAL-OFFSET GREGORIAN ANTENNA FOR THE CSU-CHILL RADAR

V. N. Bringi[1], R. Hoferer[2], D.A Brunkow[1], R. Schwerdtfeger[2], V. Chandrasekar[1], S. Rutledge[1], J. George[1] and P. C. Kennedy[1]

[1]Colorado State University, Fort Collins, Colorado
[2]GDSATCOM, Kilgore, Texas

1. INTRODUCTION

The CSU-CHILL radar has been operated as a National Facility by Colorado State University (CSU) under a cooperative agreement with the National Science Foundation (NSF) since 1990. Under the Major Research Instrumentation (MRI) program, CSU was awarded a grant to replace its prime-focus parabolic reflector antenna obtained in 1994, with a new dual-offset Gregorian design. The main objectives were to significantly improve the electrical performance of the antenna in terms of main beam symmetry, low sidelobe envelope in any plane, and to improve the cross-polar performance.

It was soon obvious that a production dual-offset design was not available for a 9 m-class main reflector and that a custom antenna had to be built by a manufacturer willing to take up the project under the MRI guidelines. VertexRSI (now GDSATCOM) located in Kilgore, TX expressed interest in building a custom 9m dual-offset antenna to very stringent specifications. At that time they had production dual-offset designs for the 4.6m-class for the SATCOM industry but the specifications (ITU-R) were not as stringent as desired by CSU. In this paper we describe the critical design features that led to a very high performance antenna for a weather radar unmatched by any other system that we are aware of at S-band. We also demonstrate, via observations, that many of the dual-polarized radar measurement artifacts that were evident with previous prime-focus parabolic reflectors, have been largely eliminated or greatly reduced especially in the presence of large reflectivity gradients.

We note that Radiation Systems Inc. (RSI) had built the original antennas for both the CHILL and CP2 radar in the early 1970s. In 1994, RSI also built the prime-focus 8.5 m parabolic antenna for CHILL which led to significant improvements in performance due to higher reflector surface accuracy and high performance feed. However, the problems associated with blockage by the feed-support spars and the feed itself (with asymmetric OMT) limited the degree of improvement that could be obtained, especially in the LDR (linear depolarization ratio) system limit (-33 to -34 dB), and the higher level of sidelobes in the planes containing the feed-support spars (45/135^o).

There are two other radars that have used the dual-offset design, (a) the C-band operational weather radar (ARPA Friuli-Venezia Giulia, Fossalon di Grado, Italy) and, (b) the K_a-band dual-offset Cassegrain design by NOAA/ETL.

*Corresponding author address: Prof. V. N. Bringi, Dept. of Electrical Engineering, Colorado State University, Fort Collins, CO 90523. email: bringi@engr.colostate.edu

2. DESIGN CONSIDERATIONS

a. Electrical (RF) performance of Feed/OMT

The basic dual-offset geometry (see Fig. 1) involves the feed/OMT (H), the 2-meter ellipsoidal sub-reflector (sector EG) and the 8.5-meter paraboloidal reflector (sector AC).

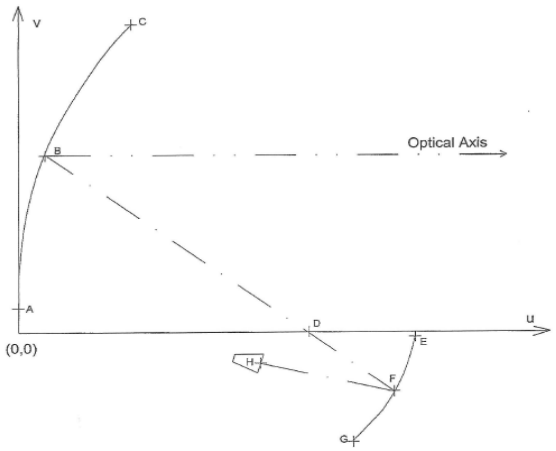

Fig 1: Basic geometry of the dual-offset Gregorian antenna.

Mizugutch et al. (1976) showed that the cross-polarized component in the aperture plane due to the asymmetrical main reflector could be cancelled out by the asymmetrical sub-reflector and by a proper geometrical arrangement with the feed. This geometrical arrangement for zero cross-polar radiation in the far-field is valid for geometrical optics only and is referred to as the Mizugutch condition which has been used in our design. Of course at

microwave frequencies where diffraction and scattering are present, the far-field cross-polarization is finite (~ -40 dB).

At the outset it was decided to design a profiled corrugated horn as shown in Fig. 2. The manufacturing tolerances for the feed were set at very 'tight' levels normally used for K-band feeds. From Olver et al. (1994), the corrugation geometry controls the cross-polar patterns, the flare angle/profile controls the copolar patterns and aperture diameter controls the copolar beam width. A symmetric OMT was chosen to achieve very high on-axis cross-polarization isolation and a very high level of port-to-port isolation. The symmetric OMT was electroformed for achieving high accuracy. Fig. 3 shows the isometric view of the OMT and the feed.

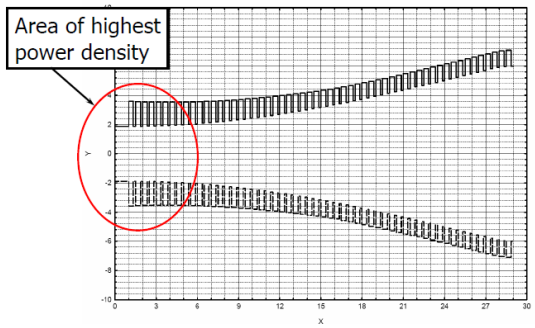

Fig. 2: Horn corrugation geometry showing area of highest power density for high power radar application. The horn aperture is 3λ in diameter.

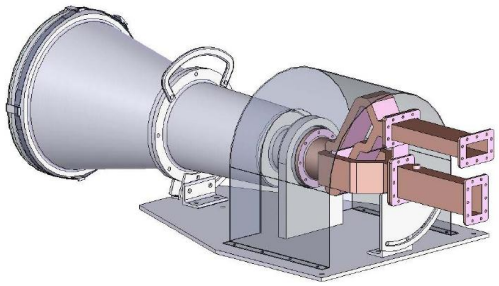

Fig. 3: Isometric view of the feed/OMT. The housing allows for rotation of the feed by 45°, effectively changing the polarization basis from nominal H-V to slant 45-135°.

Table 1 below lists the measured parameters of the symmetric OMT at the Torrance, CA facility over the 2.7-2.9 GHz band (swept frequency)

port-to-port isolation	> 58 dB
return loss (either arm)	> 24 dB
xpol isolation	> 43 dB

The specifications called for the feed copol and cross-pol patterns to be measured in the anechoic chamber at VertexRSI for the 0, 45 and 90° cuts. There were difficulties in measuring the off-axis cross-pol patterns because of limitations of the anechoic chamber as well as with fine adjustment of the source orientation with respect to the feed under test. It was then decided to independently measure the feed patterns at Ball Aerospace's much larger anechoic chamber which also allowed for 'correction' of the polarimetric errors due to the source itself (standard gain horn). However, measurement of the cross-pol patterns in the worst case plane (45°) proved inconclusive as representing the 'true' cross-pol patterns of the feed.

Fig. 4 shows the E and H plane patterns (left panel: analytical as per design) and right panel as measured in the VertexRSI anechoic chamber. The cross-pol pattern (as per design) in the 45° plane is also shown in the left panel. Fig. 4 shows that the copol amplitude patterns are in good agreement.

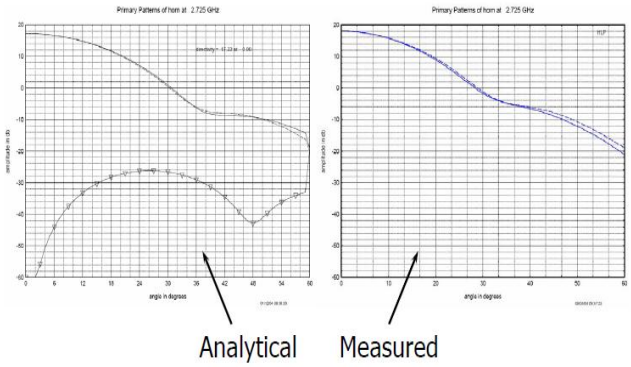

Fig. 4: Primary patterns of the feed at 2725 MHz. Left panel is per design values with xpol in the 45° plane. Right panel is from measurements in VertexRSI's anechoic chamber. Off-axis xpol could not be measured in the chamber.

The feed directivity is close to 17 dB while the taper at the sub-reflector edge is about -19 dB (30° from feed bore sight). Fig. 5 shows the corresponding phase patterns. While the shapes are generally similar, the disagreement is due to the phase center of the feed being intentionally displaced 4" inward from the 'true' focus. This was done to 'shoulder-in' the theoretical first side lobes into the main beam (far-field patterns to be shown later). Thus, the measured phase patterns in Fig. 5 are 'sloped down' as the horn moves towards the sub-reflector.

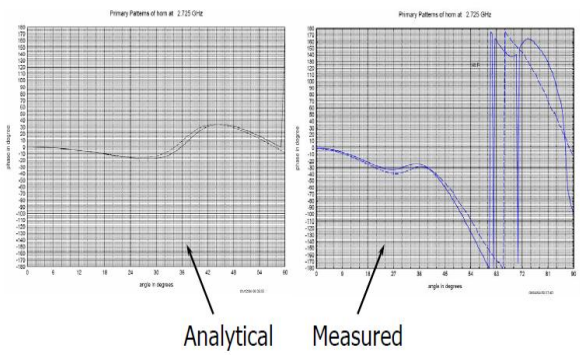

Fig. 5: As in Fig. 4 except phase patterns are shown.

The feed/OMT was brought to the CSU-CHILL site for high power testing after simulations predicted that the maximum electric field would occur in the OMT with a predicted safety margin of 22% (assuming 9 psi pressurization and 2 dB waveguide loss). The high power testing of the feed/OMT was successful.

b. Main reflector

The 8.5-meter main reflector consists of 20 panels in three tiers as shown in Fig. 6. The panel gaps were designed to be 1/16" as opposed to the more common gap of 1/8".

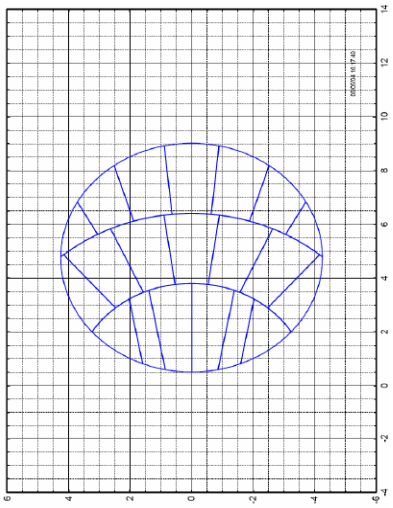

Fig. 6: The 20 panels forming the main reflector in 3 tiers.

This was done to reduce any cross-polarized component of edge currents along the gaps. Each panel was made from two stretch-formed aluminum skins bonded on each side of an aluminum honeycomb core to give very high stiffness to weight ratio. The surface accuracy of each panel is around 2 mil (rms). For disassembly and transport as per design requirements, the reflector comes apart in three sections after 6 panels are removed (see Fig. 7). This was done to avoid any linear vertical cuts in the panels which was found to produce unacceptably enhanced cross-polarized component of the edge currents. The 2-meter ellipsoidal sub-reflector was constructed via a machined aluminum casting with surface accuracy of 2 mil (rms).

The far-field predictions were made with TICRA software (www.ticra.com). The measured feed copol patterns and the analytical cross-pol patterns as per Figs. 4 and 5 were used as input.

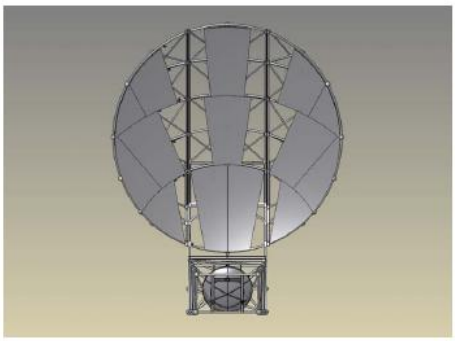

Fig. 7: Main reflector panels showing the 6 removable panels prior to disassembly into three sections for transport.

The spherical wave function expansions (SWE) of the measured feed data were used since the sub-reflector is in the near-field of the feed. Such a SWE representation of the primary feed pattern produces a more accurate prediction of the side lobes especially those in the sub-reflector 'back lobe' region (roughly 20-40° from main beam bore sight). The 20 panels with gaps were used as input along with the sub-reflector and the geometry as in Fig. 1. These far-field predictions were important bench marks for CSU and were used to establish that the antenna satisfied the critical design review part of the contract.

3. RANGE TESTS

The completed antenna was tested at VertexRSI's has a long range pattern measurement facility shown in Fig. 8. Note that the elevation angle to the flat plate on the top of the tower is 1.8°. The specifications called for range probing using a standard gain horn mounted on a 27' long probe carriage to map the field across the test aperture. In the azimuth plane there were 'slow' variations across the test aperture in the range ± 1 dB (regardless of polarization i.e., H or V), whereas in the elevation plane, 'fast ripple' interference patterns showed variations as large as ± 5 dB for both H and V polarizations. Regarding the cross-pol of the source itself, three points were noted, (i) the source antenna is located at the bottom of the tower, (ii) the asymmetry that is present between the source feed and the flat reflector at the top of the tower (Fig. 8), and (iii) the polarization effects of the uneven ground between the tower and the test antenna positioner. Hence, the long range facility was

mainly used to validate the main beam symmetry and copol side lobe envelope specifications with patterns cut in the azimuth (narrow angle of ± 45° and wide angle of ± 180°) and elevation planes (-1.5 to 90°) with the antenna under test (AUT) at orientations of 0, ± 45 and 90°.

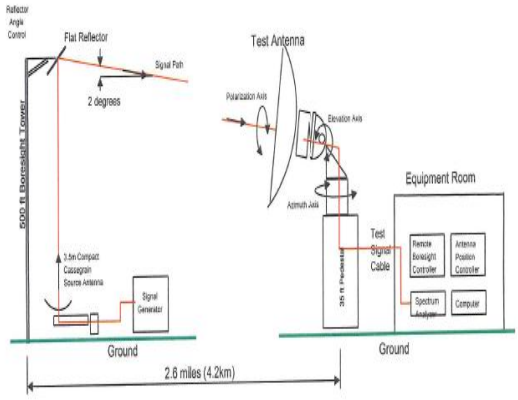

Fig. 8: Long range test facility in Kilgore, TX used for wide angle azimuth patterns (mainly copol) with antenna under test (AUT) at orientations of 0, 45, -45 and 90°.

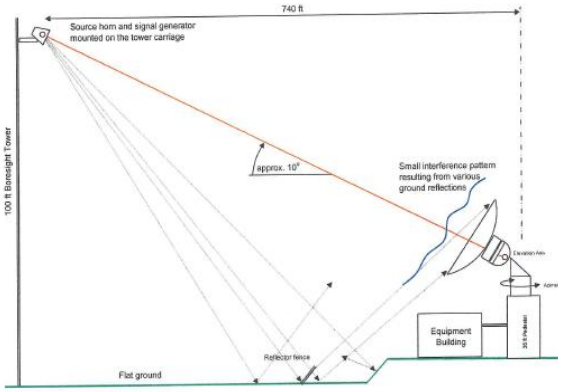

Fig. 9: Short range test facility used mainly for narrow angle elevation patterns (for cross-pol). Source horn is identical to the feed constructed for the antenna under test.

For validation of the cross-pol pattern specifications it was decided to use the short range test facility shown in Fig. 9 where the elevation angle to the source is close to 12°. The source feed was made identical to the feed for the antenna under test to minimize the cross-pol radiated by the source. All patterns were made in the elevation plane (-1.5 to 10° relative to beam center) with the antenna under test (AUT) at orientations of 0, ± 45, ± 90, ± 135 and 180°.

A comprehensive range test plan was executed using both the long and short range test facilities with a total of more than 40 pattern cuts to fully characterize the test antenna. Only a few sample patterns will be shown here for illustration. First we show some examples of copol patterns using the long range facility with Fig. 10 showing the wide angle azimuthal plane pattern (±180°). The side lobe envelope specification (drawn in) was -33 dB at 2° to -50 dB at 10° with logarithmic variation with angle (θ), and < -50 dB from 10 to 180°. Equivalently, it is expressed as (relative to peak gain which is 45.5 dBi):

Envelope = $20.8-25.8 \log_{10}(\theta)$ dBi for $2<\theta<10^{\circ}$

<-5 dBi for $10<\theta<180^{\circ}$

Local peak deviations of <2 dB above the specified envelope were allowed for $2<\theta<10^{\circ}$, and up to 5 dB for $\theta>10^{\circ}$: the latter was to accommodate the sub-reflector 'spill over' angular region seen in Fig. 10 for θ in the interval 30-50°.

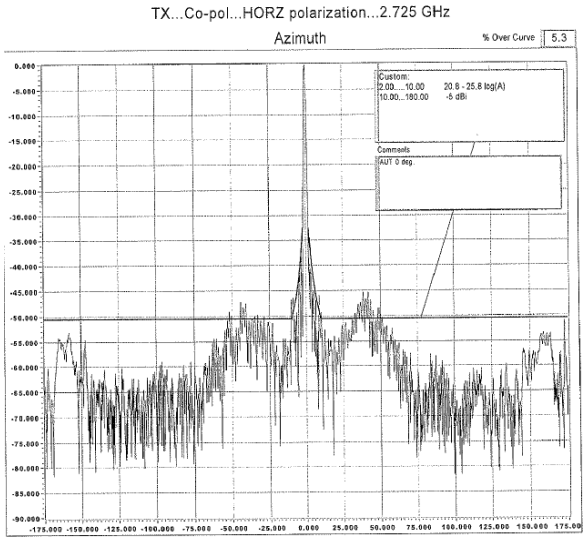

Fig. 10: Wide angle (± 175°) azimuth plane cut using the long range facility. Source is at H polarization and antenna under test (AUT) is at 0° orientation (as in Fig. 7), i.e. the copol pattern.

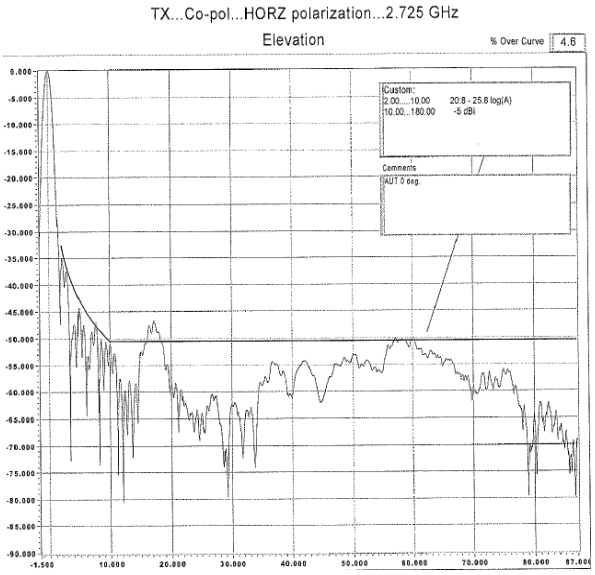

Fig. 11: As in Fig. 10 except elevation cut from -1.5 to 87°.

Fig.11 shows the elevation cut as in Fig. 10 where the side lobe envelope is more clearly seen. Fig. 12 shows the azimuth cut with the AUT orientation at -45°. The angular interval is between -45 to 45°.

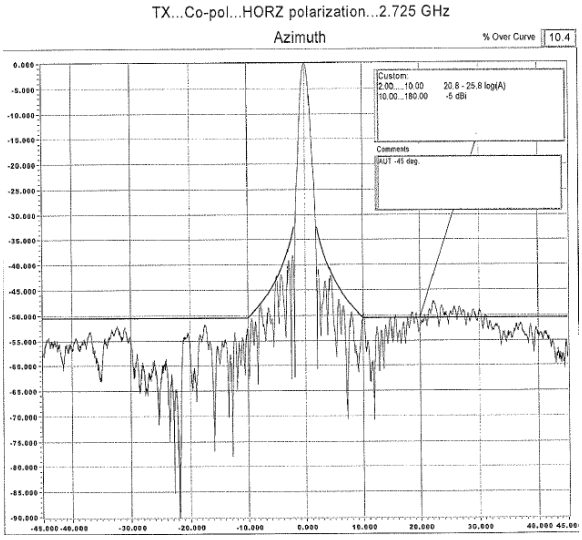

Fig. 12: As in Fig. 10 except AUT orientation at -45° and narrower angular interval [-45,45°].

We now show cross-polar patterns taken in the short range facility. As mentioned before, all patterns were cut in the elevation plane only. The specifications for the cross-polar pattern were: on-axis xpol < -43 dB and off-axis xpol <-35 dB for 0<θ<2°. Beyond 2° the xpol should be <-45 dB. Figs. 13-15 show the patterns with the AUT at orientations of 0, -45 and -90°.

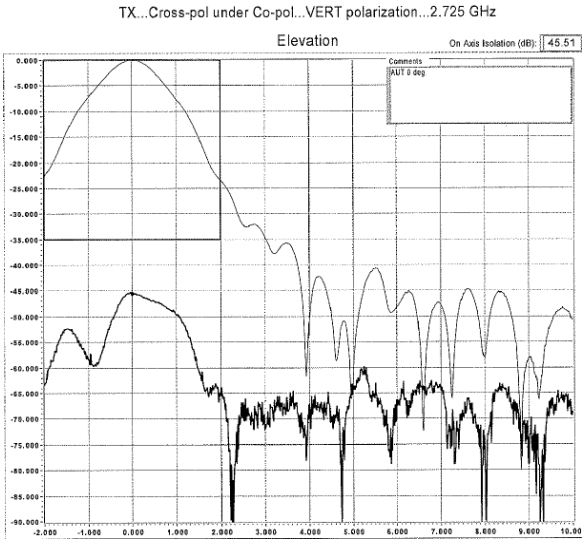

Fig. 13: Elevation cut with AUT oriented at 0° (as in Fig. 7). Angular extent of the pattern is -2 to 10°. The on-axis xpol is -45.5 dB.

Note that with the AUT oriented at 0°, the off-axis xpol will be, in theory, negligible but in practice will mimic the copol main lobe for small angles. One can see this to some extent in Fig. 13. The copol pattern will be in the near-field and its main lobe will 'appear' wider.

Figs.14 and 15 show similar elevation plane cuts with AUT oriented at -45 and -90°. As can be seen the xpol patterns now have a minima on-axis and the off-axis peaks are symmetrically placed within -2 to 2°.

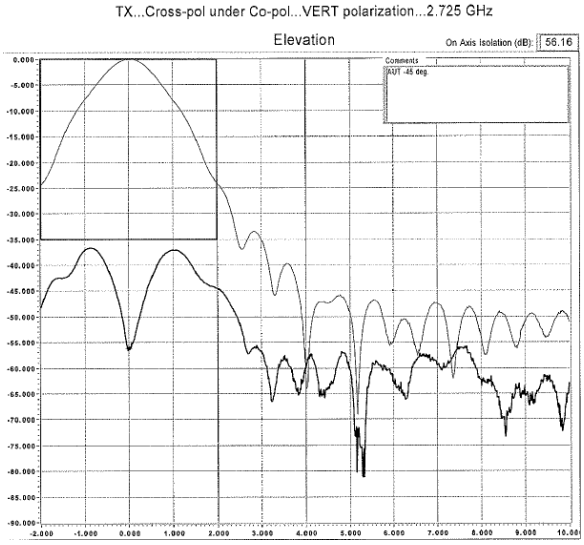

Fig. 14: As in Fig. 13 except AUT oriented at -45°. The on-axis xpol is -56 dB and the peak off-axis xpol is -37 dB.

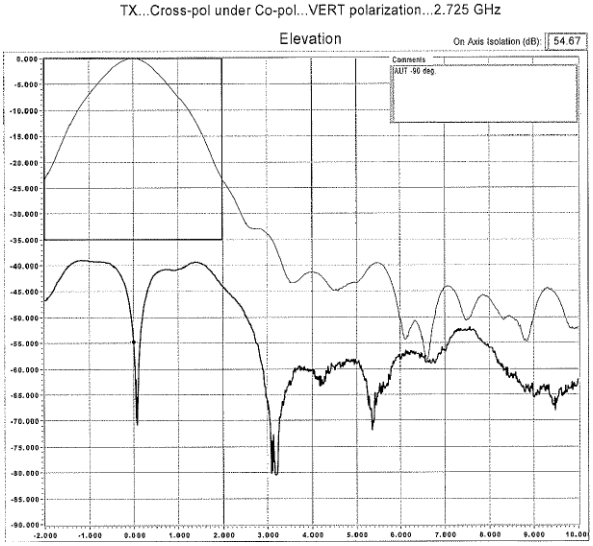

Fig. 15: As in Fig. 13 except AUT oriented at -90°. The on-axis xpol is -54 dB and the peak off-axis xpol is -39 dB.

Examination of the xpol patterns showed that the worst case off-axis xpol occurred in the 45/135° planes in agreement with theory. For some of the patterns, with the AUT at ± 45° orientation, the peak off-axis xpol specification was missed occasionally by several dB but not when the AUT was at ± 135°. This might have occurred because the feed support boom was closer to the top of the equipment building (see Fig. 9) when the AUT was oriented at ± 45° as opposed to ± 135° (for reference Fig. 7 shows the AUT at 0° orientation and Fig.16 shows photo of antenna in 135º position on the test range). Hence we took the patterns at ± 135° as being closer to the actual performance and deemed to have met the specifications at all AUT orientations.

The antenna was installed on the CSU-CHILL pedestal in early 2008. After installation a photogrammetry method was used to establish the main reflector surface accuracy (0.016" rms as opposed to the specification of 0.02") and to precisely align the geometry as per the design drawings. Table 2 lists the antenna characteristics. The linear depolarization ratio (LDR) system limit of -40 dB was based on data collected in light stratiform rain as will be shown in the next section.

Fig. 16: Antenna in 135º position on the test range.

4. MEASUREMENTS

Ultimately the antenna performance must be determined via measurements and whenever possible, substantial reduction in measurement artifacts due to high gradients must be shown over the previous prime-focus 8.5 m reflector antenna. Several performance measures were considered among them (i) the system LDR limit in light stratiform rain, (ii) reduction in cross-beam, gradient-induced artifacts, especially in Z_{dr}, Φ_{dp} and ρ_{co} , (iii) improvement in data quality due to greatly reduced clutter power entering via the side lobes.

a. Stratiform rain with embedded convection

To illustrate the quality of the recently acquired measurements with the new antenna, we show data acquired from one low elevation angle sweep at short ranges (range from 5 to 30 km; azimuth sector from 105-180°) in stratiform rain with embedded convection which occurred on June 5, 2008. The CSU-CHILL radar was operated in the alternating (VH) mode with the two transmitters firing alternately. The copol signals are routed to the copol receiver and similarly with the xpol signals. Fig. 17 shows the PPI sweep of reflectivity at elevation angle of 1.5 deg.

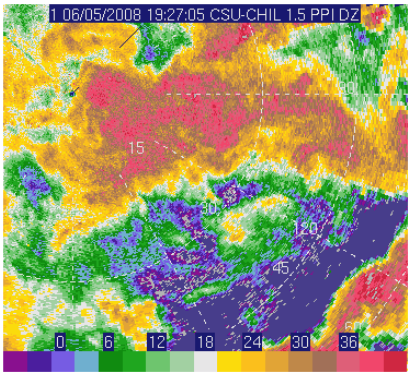

Fig. 17: PPI of reflectivity (Z_h) at 1.5° elevation angle in stratiform rain with embedded convection.

To set the baseline for the data quality we show in Fig. 18 the color-filled plot of Z_{dr} versus Z_h with frequency of occurrence of pairs of (Z_h,Z_{dr}) shown on a logarithmic scale. The Z_h data were recorded with 3/8th dB steps and for Z_{dr} it was 3/16th dB. However, the powers have been recorded with much greater precision (double-precision floating point). The data shown are from each 150 m range gate and have been clutter filtered. The Z_{dr} data has also been corrected for receiver noise. A data mask has been applied for each beam using the standard deviation of φ_{dp} over 10 consecutive gates with values < 5° being classified as 'meteo' echoes. The variation of Z_{dr} with Z_h falls well within the bounds expected from scattering simulations based on DSDs at S-band. For example, such data can be used to describe 2D-membership functions for fuzzy-logic methods of hydrometeor classification.

The histogram of *LDR* for this dataset is shown in Fig. 19 which indicates that the mode for stratiform rain appears to be -35 dB; it also indicates that the system *LDR* limit is close to or better than -40 dB (a good 7 dB improvement over the previous prime-focus fed parabolic reflector antenna).

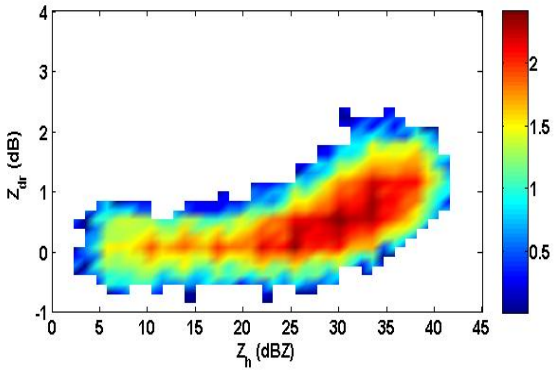

Fig. 18: Plot of Z_{dr} versus Z_h shown as frequency of occurrence of the pairs in a log scale.

Table 2: Antenna Characteristics

Type	Dual-offset Gregorian
Frequency	2725-2875 MHz
3-dB beam width	0.97°
Gain	45.5 dB
Main reflector surface accuracy	0.016" (measured on site)
Polarization basis	H-V or slant 45°-135°
Feed	profiled corrugated horn
Orthomode transducer	symmetric
On-axis cross-pol	< -43 dB
Peak off-axis cross-pol	< -35 dB in any plane
Side lobe envelope	$-25.7-24.3\log_{10}(\theta)$: 2<θ<10° <-50dB 2<θ<180° *[< -45 dB in sub-reflector spillover angles ~ 30-50°]*
LDR system limit from data	-40 dB or better

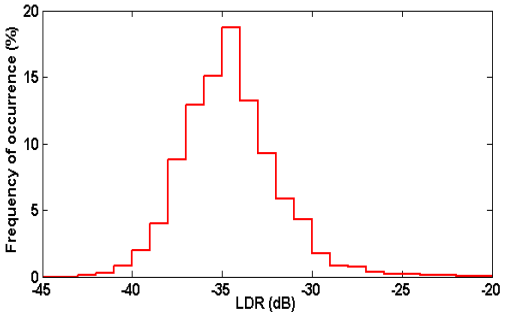

Fig. 19: Histogram of *LDR* in stratiform rain with embedded convection.

To illustrate the high quality of the copolar correlation coefficient (ρ_{co}) we show in Fig. 20 the plot of ρ_{co} (%) versus Z_h noting that the normalizing powers in the expression for ρ_{co} have not been corrected for receiver noise. Hence, the drop off in ρ_{co} for Z_h<15 dBZ. Otherwise, the values are very high approaching 0.995 or higher. This is further illustrated in the histogram shown in Fig. 21 with the mode close to 0.997 (99.7%).

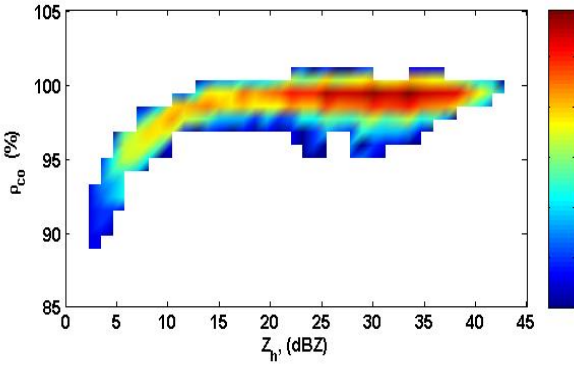

Fig. 20: Plot of ρ_{co} versus Z_h with the fall off for Z_h<15 dBZ due to not correcting the normalizing powers (H and V) for receiver noise.

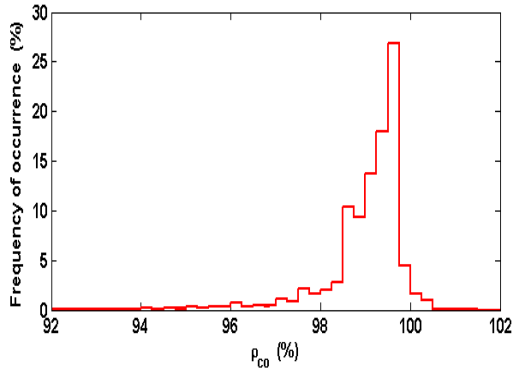

Fig. 21: Histogram of ρ_{co} . Note mode close to 99.7 %. A few occurrences >100% are due to the alternating mode algorithm which assumes Gaussian Doppler spectrum.

b. Thunderstorm RHI observations

Antenna test data were also collected during severe thunderstorm conditions shortly after 00 UTC on June 21, 2008. The copol reflectivity field is shown in Fig. 22. The echo summit is clearly depicted without the sidelobe "smears" that were commonly observed with the center fed antenna.

The corresponding differential reflectivity data is shown in Fig. 23. Other than a globally-applied bias correction, no additional thresholding or editing has been applied to the data. Apparent Z_{dr} artifacts are restricted to a small, low SNR area near X=43, Z=7 km.

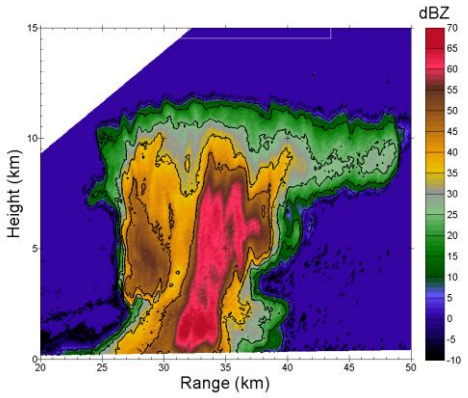

Fig. 22. Reflectivity field at 0146:00 UTC on June 21, 2008.

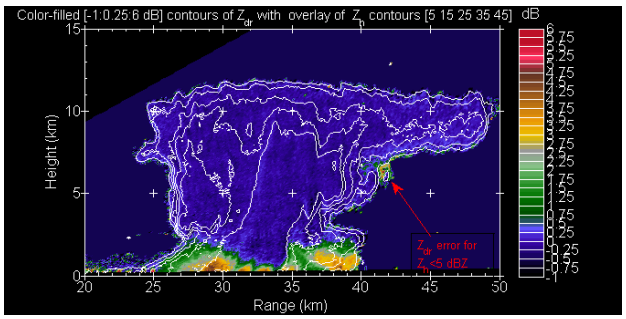

Fig. 23: Differential reflectivity (color fill) and reflectivity contours at 0146:00 on June 21, 2008. Arrow marks apparent Z_{dr} field artifact.

Finally, the differential propagation phase field from this same RHI sweep is shown in Fig. 24. The ϕ_{dp} trends with range show no evidence of corruption in high reflectivity gradient regions.

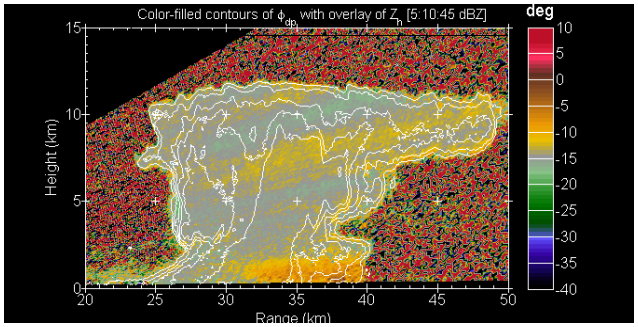

Fig. 24: Differential propagation phase (color fill) and reflectivity contours at 0146:00 on June 21, 2008.

c. Gust front in clear air echo

Due to the low sidelobe levels achieved by the dual offset feed antenna, ground clutter contamination decreases rapidly with increasing antenna elevation angle. The following RHI scans were made through

the fine line echo associated with a thunderstorm gust front that was nearing the radar site. Reflectivity levels were generally quite low in the boundary layer. Nevertheless, the shallow inbound radial velocity pattern is clearly sampled down to heights immediately adjacent to the strong ground returns.

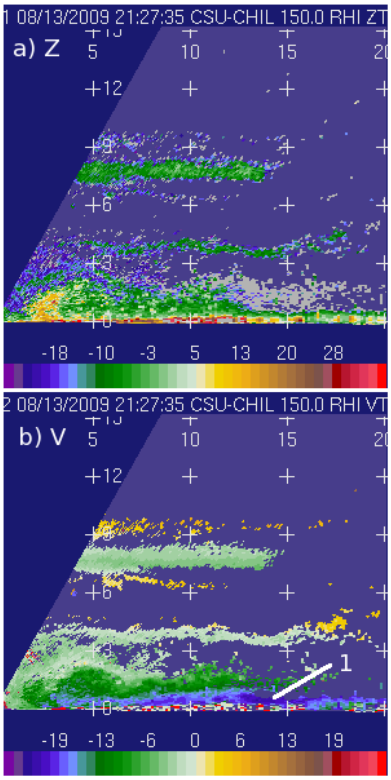

Fig. 25: RHI scan through an approaching gust front on August 13, 2009. (a) Reflectivity (dBZ); (b) Radial velocity (ms^{-1}; negative sign for approaching motion). Point 1 marks the maximum velocity layer located near the surface.

References

Mizugutch, Y., M. Akagawa and H. Yokoi, 1976: Offset dual reflector antenna, IEEE AP-S Int. Symp. Digest, pp 1-5, Oct 1976.

Olver, A.D., P.J.B. Clarricoats, A.A. Kishk and L. Shafai, “Microwave Horns and Feeds”, IEE Electromagnetic Waves Series 39, IEE UK and IEEE New York, pp 490.

Acknowledgments

The CSU-CHILL National Radar facility is supported by NSF ATM 0735110. The new antenna acquisition was made possible by a Major Research Instrumentation grant from the U.S. National Science Foundation (NSF) via ATM 0216192. GDSATCOM provided cost-sharing funds of 15% for design and range testing. CSU is grateful to Dr. P. Ramanujam for his contributions during the preliminary and critical design reviews.

In Memoriam

Dr. Raj Chugh was instrumental in the RF design of the very low cross-pol dual offset antenna system described in this paper. Sadly, near the end of the project, he passed away at the age of 58 on 23 May 2005, yet to be remembered by all involved. Rajinder Kumar Chugh was born in District Kamaliya Layalpur, Pakistan on 2 November 1946. He received his BEE from the Indian Institute of Technology (IIT) in New Delhi, and then his PhD in electromagnetics at the University of Manitoba in Canada. After several professional adventures, he came to Vertex Communications Corp (now General Dynamics) in 1984 as Principal Scientist. Raj's understanding and computational carefulness were his highly recognized trademarks - everything was always correct.